

360° High-Resolution Depth Estimation via Uncertainty-aware Structural Knowledge Transfer

Zidong Cao, Hao Ai, Athanasios V. Vasilakos, *IEEE Senior Member*, Lin Wang[†], *Member, IEEE*

Abstract—To predict high-resolution (HR) omnidirectional depth maps, existing methods typically leverage HR omnidirectional image (ODI) as the input via fully-supervised learning. However, in practice, taking HR ODI as input is undesired due to resource-constrained devices. In addition, depth maps are often with lower resolution than color images. Therefore, in this paper, we explore for the first time to estimate the HR omnidirectional depth directly from a low-resolution (LR) ODI, when no HR depth GT map is available. Our key idea is to transfer the scene structural knowledge from the HR image modality and the corresponding LR depth maps to achieve the goal of HR depth estimation without any extra inference cost. Specifically, we introduce ODI super-resolution (SR) as an auxiliary task and train both tasks collaboratively in a weakly supervised manner to boost the performance of HR depth estimation. The ODI SR task extracts the scene structural knowledge via uncertainty estimation. Buttressed by this, a scene structural knowledge transfer (SSKT) module is proposed with two key components. First, we employ a cylindrical implicit interpolation function (CIIF) to learn cylindrical neural interpolation weights for feature up-sampling and share the parameters of CIIFs between the two tasks. Then, we propose a feature distillation (FD) loss that provides extra structural regularization to help the HR depth estimation task learn more scene structural knowledge. Extensive experiments demonstrate that our weakly-supervised method outperforms baseline methods, and even achieves comparable performance with the fully-supervised methods.

Impact Statement—Our weakly-supervised can adapt to various backbones, input sizes, and datasets. Our method can also easily be applied to higher resolution, such as 1024×2048 . We contribute the effectiveness to the proposed SSKT module, which successfully transfers essential scene structural knowledge from the ODI SR task to the HR depth estimation task. Importantly, we prove that the way of transferring the scene structural knowledge from the HR image modality and corresponding LR depth map is feasible to achieve the goal of HR depth estimation without any extra inference cost.

Index Terms—Omnidirectional image, depth estimation, image super-resolution, knowledge transfer, weakly-supervised learning

I. INTRODUCTION

Monocular depth estimation is a fundamental task of 3D scene understanding that finds its applications in various fields, such as autonomous driving. The advancements in deep

Z. Cao, H. Ai are with the Artificial Intelligence Thrust, The Hong Kong University of Science and Technology (HKUST), Guangzhou, China. E-mail: {caozidong1996@gmail.com, hai033@connect.hkust-gz.edu.cn}

Athanasios V. Vasilakos is with the Center for AI Research (CAIR), University of Agder(UiA), Grimstad, Norway. Email: thanos.vasilakos@uia.no

L. Wang is with the Artificial Intelligence Thrust, HKUST, Guangzhou, and Dept. of Computer Science and Engineering, HKUST, Hong Kong SAR, China. E-mail: linwang@ust.hk.

[†]Corresponding author

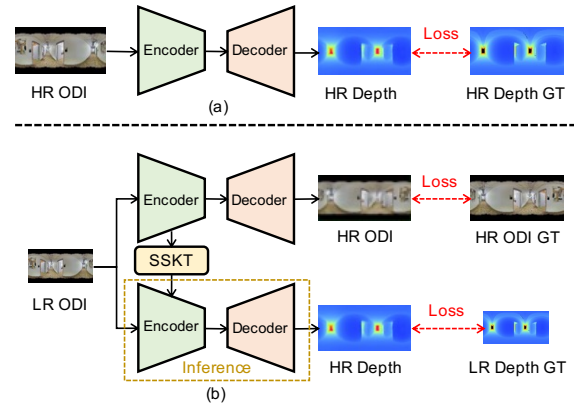


Fig. 1. HR depth estimation paradigms. (a) Existing fully-supervised methods. (b) Our weakly-supervised method transfers knowledge between two tasks via the SSKT module.

neural networks (DNNs) [1] and the accessibility of large-scale annotated datasets have resulted in notable improvements in monocular depth estimation. Nevertheless, most of the existing approaches are developed for perspective images, which suffer from a limited field-of-view (FoV) [2], [3].

Recently, 360° cameras¹ have received considerable attention because of their ability to capture the environment with a wide FoV of $180^\circ \times 360^\circ$ in a single shot. Omnidirectional images (ODIs)² present the scene entirely with rich scene contexts. This distinct advantage has inspired active research for monocular depth estimation [4]–[7]. However, the angular resolution of ODIs is relatively lower than that of perspective images when ODIs and perspective images are captured by different sensors with identical sizes. The low angular resolution leads to degraded structural details such as edges, rendering it difficult for omnidirectional depth estimation.

To reconstruct the structural details, existing methods [5]–[13] leverage high-resolution (HR) ODIs as inputs with the supervision of HR depth ground truth (GT) maps. For instance, using the HR ODIs and paired HR depth GT maps, OmniDepth [9] employs the encoder-decoder architecture to predict HR depth maps, as shown in Fig. 1(a). However, in practice, taking HR ODI as input is undesired by resource-constrained devices. Take virtual reality (VR) as an example, the headsets often have limited bandwidth for transmission and limited computational resources [14]. Processing HR ODIs in the headsets might cause high latency due to limited bandwidth [14]. In addition, obtaining HR depth maps is arduous and expensive [15]. This is because depth sensors, such as LiDARs, often capture sparse depths with low resolution [16].

¹Also called omnidirectional cameras.

²ODIs usually indicate the equirectangular projection (ERP) type images.

Also, increasing the lens of LiDARs is far more expensive than obtaining HR ODI [17].

Motivation. In this paper, we explore for the first time to estimate the HR depth map directly from an LR ODI, when no HR depth GT map is available (See Fig 1(b)). Without the supervision of HR depth GT maps, the fine scene structural details can scarcely be recovered in the HR depth predictions. Therefore, to explore valuable supplementary supervision that can facilitate HR depth estimation, our key idea is to learn and transfer scene structural knowledge from the HR image modality and the corresponding LR depth maps to achieve the goal of HR depth estimation without causing extra inference cost. This is inspired by the fact that **1**) there exists publicly available large-scale LR-HR paired image datasets and thus achieve the super-resolution (SR) task [18]–[22]; **2**) an ODI and its corresponding depth map are photometric and geometric representations of the same scene, respectively [15]. This implies that both representations share the common scene structural knowledge, such as edges.

Specifically, we employ the ODI SR as an auxiliary task and train both tasks collaboratively in a weakly-supervised manner to boost the performance of HR depth estimation. The ODI SR task takes an LR ODI as input to predict a super-resolved RGB image. As the textural details in the super-resolved RGB image may interfere with the smoothness of depth prediction [5], [23], we introduce uncertainty estimation [24] for the ODI SR task to specially extract the scene structural knowledge. The high-uncertainty regions are often matched with high-frequency regions, which can be utilized to emphasize the regions carrying more structural knowledge [24]. Upon this, we propose a scene structural knowledge transfer (SSKT) module with two key components.

Firstly, considering the unique properties of the equirectangular projection (ERP) type of ODIs, we design a novel cylindrical implicit interpolation function (CIIF) for feature up-sampling by learning the neural interpolation weights based on cylindrical coordinates. This way, our CIIF alleviates the discontinuity and stretched distortion of ODIs. Also, as the learned interpolation weights can capture the correlations among neighboring pixels, they can be used to represent the scene structural knowledge. Therefore, by sharing the parameters of CIIFs between the ODI SR and HR depth estimation tasks, structural knowledge can be transferred between the two tasks effectively. Secondly, as the features of the ODI SR task also contain crucial scene structural knowledge, we propose a feature distillation (FD) loss to refine depth estimation.

In total, our weakly-supervised method is *efficient*, as the ODI SR network and SSKT module can be removed freely and only LR ODI is needed during inference, introducing no extra inference cost. Moreover, our method is *flexible* and can be easily adapted as a plug-and-play approach by modifying the backbones for the HR depth estimation network and varying the up-sampling factors (See Tab. I). Furthermore, we demonstrate the *effectiveness* of our method across different datasets [9], [25], [26], with various up-sampling factors and backbones. The experimental results show that our method not only *outperforms* the baseline methods, but also achieves *comparable* performance with the fully-supervised methods.

Our main contributions can be summarized into four-fold:

- We propose the first weakly-supervised method that predicts the HR omnidirectional depth map from an LR ODI when no HR depth GT map is available.
- We propose to learn and transfer the scene structural knowledge from an uncertainty-driven ODI SR task.
- We propose an SSKT module with two components. The first is the CIIF as it is specific for ODIs to learn neural interpolation weights. The second is the FD loss to provide extra structural regularization.
- Experimental results demonstrate that our proposed method is efficient, flexible, and effective, which achieves comparable results with the fully supervised methods.

II. RELATED WORK

Omnidirectional Monocular Depth Estimation. Some attempts have been made to tackle the spherical distortion in ODIs by modifying the characteristics of convolutional filters, including row-wise rectangular filter [9], deforming the sampling grids [11], and dilated convolutions for larger receptive fields [12]. Another direction is to combine different projection types, *e.g.*, ERP, cube map [5], [7], and tangent projection [8], [27]. BiFuse [7] proposes a bi-projection fusion model for the ERP images and cube maps to share information with each other, while UniFuse [5] demonstrates that the unidirectional fusion from the cube map to ERP is more effective. Some methods [10], [13] focus on parallel computation in omnidirectional monocular depth estimation. The typical pipeline is first projecting an ERP image into multiple low-resolution perspective patches, then predicting depth maps in parallel, and finally re-projecting the perspective depth predictions back to the ERP plane. Recently, Li *et al.* [28] propose to extract features on the unit sphere to relieve the distortion effect. However, all the aforementioned methods require HR depth maps for supervision.

Omnidirectional image super-resolution. Cagri *et al.* [29] propose the first DNN-based framework via adversarial learning. LAU-Net [18] addresses the non-uniformly distributed pixel density of the ERP type ODI via adaptively up-sampling different latitude bands. SphereSR [19] proposes a continuous spherical representation to model the sphere as an icosahedron and reconstruct ODIs with multiple projection types.

Modeling Uncertainty in image super-resolution. In the image SR task, high-frequency regions with rich texture and edges carry more visual information than the smooth regions [24]. To better capture the high-frequency details and emphasize the corresponding pixels, some uncertainty-driven image SR methods have been proposed [24], [30]. For instance, GRAM [30] extracts the uncertainty map via the Gaussian assumption and takes the uncertainty map as the attenuation mask to achieve better performance. Differently, Ning *et al.* [24] estimate the uncertainty with Jeffrey’s prior and proposes an uncertainty-driven loss to provide attention for the pixels with high uncertainty. Our method introduces the uncertainty estimation to extract scene structural knowledge, which is transferred to the depth estimation task.

Implicit Neural Representation. For the image SR task, Chen *et al.* [31] propose an implicit function, LIIF, to represent

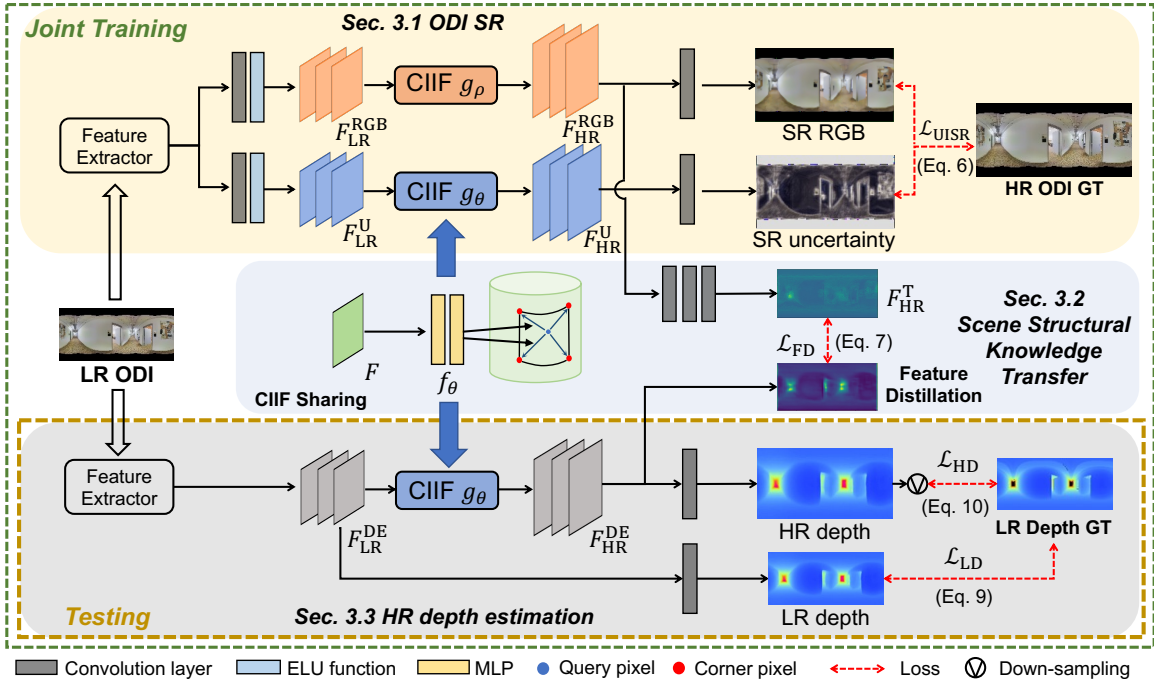


Fig. 2. **Overview of our weakly-supervised framework.** Firstly, we introduce an ODI SR task (Sec III-A) which predicts uncertainty to extract structural knowledge. Then, we design an SSKT module with CIIF that learns cylindrical neural interpolation weights and shares parameters between the two tasks. The SSKT module also includes an FD loss (Sec III-B) for feature distillation. Finally, we employ an HR depth estimation task (Sec III-C) to generate HR depth estimation directly from an LR ODI. The detailed components of CIIF is shown in Fig. 3(b).

images continuously and achieves the up-sampling process with arbitrary factors. Furthermore, Tang *et al.* [32] replace the non-parametric interpolation weights in LIIF with the ones learned from the input image and depth map to achieve the guided depth SR task. However, the mentioned two implicit functions [31], [32] are based on the Cartesian coordinate system, which is weak in tackling the discontinuity and distortion problems in the ERP type ODIs. In contrast, our proposed CIIF is constructed based on cylindrical coordinates, which is effective in alleviating the mentioned problems in ERP type ODIs, as evaluated in Tab. IV.

Multi-task learning. It is mainly used for correlated tasks [33] or domains [34]–[36]. Wang *et al.* [37] treat image SR as an auxiliary task for semantic segmentation with full supervision. Sun *et al.* [15] leverage the monocular depth estimation task to facilitate the depth SR task, reconstructing finer details.

III. METHOD

Overview. The goal is to predict an HR omnidirectional depth map D_{HR} from an LR ODI I_{LR} as input, using only an LR depth map D_{LR}^{GT} for supervision. As shown in Fig. 2, our framework consists of an ODI SR task, a scene structural knowledge transfer (SSKT) module, and an HR depth estimation task. The ODI SR is employed as an auxiliary task and trained collaboratively with the HR depth estimation task. Specifically, we introduce uncertainty estimation to the ODI SR task for scene structural knowledge extraction. To transfer the extracted knowledge, the SSKT module is proposed with two components. The first is to share the parameters of the proposed cylindrical implicit interpolation function (CIIF) between the two tasks. The second is the feature distillation (FD) loss that provides extra structural regularization. The

overall training process can be seen in Algorithm. 1. We now describe the components in detail.

A. ODI SR

The omnidirectional images contain not only the complete structural details of the surroundings but also rich textural details in the scenes. However, the enriched textural details can interfere with the smoothness of predicted depth maps [5], [6], [23]. Therefore, directly transferring knowledge from the ODI SR task degrades the depth estimation performance (See Tab. III). Inspired by the recent progress of uncertainty-driven image super-resolution [24], which demonstrates that regions with high uncertainty are often matched with high-frequency regions, we introduce the uncertainty estimation to the ODI SR task. By doing so, the regions that carry more structural knowledge can be emphasized, which is beneficial to reconstruct more structural details in the HR depth estimation task. Specifically, as shown in Fig. 2, we utilize the feature extractor to process the LR ODI I_{LR} and utilize two groups of convolutional layers with ELU activation functions [38] to output LR features for the RGB part F_{LR}^{RGB} and uncertainty part F_{LR}^U , respectively. Then, F_{LR}^{RGB} is up-sampled by CIIF with parameters g_ρ to generate HR features F_{HR}^{RGB} . Similarly, F_{LR}^U is up-sampled by CIIF with parameters g_θ to generate HR features F_{HR}^U . We then describe the components of CIIF that achieve the feature up-sampling process.

CIIF. Generally, the image interpolation problems can be defined as follows:

$$I_{HR}(x_q) = \sum_{i \in N_q} w_{q,i} I_{LR}(x_i), \quad (1)$$

where x_q is the coordinate of query pixel q in the HR image domain, x_i is the coordinate of corner pixel i in the LR image

domain; N_q represents the neighboring pixels of q in the LR image domain and $w_{q,i}$ is the interpolation weight between pixel q and i . We take LIIF [31] as an example to illustrate the interpolation process, depicted in Fig. 3(a). In LIIF, given the latent code z_i encoded from I_{LR} and the coordinate relation between q and i , the RGB value of q in the HR image domain is predicted by the MLP f_θ with parameters θ as follows:

$$I_{HR}(x_q) = f_\theta(z_i, x_q - x_i). \quad (2)$$

To address the border discontinuity issue, LIIF [31] averages the four predictions of query pixel q from its four corner pixels. Notably, the interpolation weight $w_{q,i}$ is calculated by the partial area S_i diagonally opposite to the corner pixel i (See Fig. 3(a)). Thus, Eq. (2) can be extended to:

$$I_{HR}(x_q) = \sum_{i=1}^4 \frac{S_i}{\sum_{i=1}^4 S_i} f_\theta(z_i, x_q - x_i). \quad (3)$$

Furthermore, [32] replaces the scale factor S_i in Eq. (3) with learnable interpolation weights to obtain smoother results. However, for ODIs with ERP type, which unfolds from the sphere in a cylindrical manner, there are two specific challenges: 1) The discontinuity between the left and right sides; 2) The stretched distortion toward the poles (the top and bottom of ODIs). Previous implicit interpolation methods, *e.g.* [31], [32], are based on the Cartesian coordinate, which is less effective in representing spatial correlation of pixels in ODIs [19]. Therefore, we propose to reframe ODIs with the cylindrical representation, as shown in Fig. 3(b). The cylindrical angle coordinate is formulated as $\alpha \in (-\arctan(\frac{\pi h}{w}), \arctan(\frac{\pi h}{w}))$ (Latitude angle), $\beta \in (-\pi, \pi)$ (Longitude angle). For the calculation of the cylindrical representation, we recommend readers to refer to the first section of the supplemental material. Based on the cylindrical angle coordinate, we learn the cylindrical implicit interpolation weights (See Fig. 3(b)):

$$w_{q,i} = g_\theta(z_i, (\alpha_i - \alpha_q, \beta_i - \beta_q)). \quad (4)$$

After obtaining the interpolation weights $w_{q,i}$ in Eq. (4), we combine the weights $w_{q,i}$ with latent code z_i from the LR feature F_{LR} to obtain an HR feature F_{HR} . Finally, the HR features are processed with two different convolutional layers to output the super-resolved RGB image (*i.e.*, mean) μ_{HR} and super-resolved uncertainty map (*i.e.*, variance) σ_{HR} , respectively. Formally, by assuming that uncertainty meets the Laplace distribution, an HR ODI is described as:

$$I_{HR} = \mu_{HR} + \epsilon \times \sigma_{HR}, \quad (5)$$

where ϵ represents the Laplace distribution with the zero mean and unit variance. Specifically, we employ the first stage of [24] with the maximum likelihood estimation (MLE). For stable training, we utilize the logarithmic form of uncertainty $s = \log \sigma_{HR}$. The uncertainty-driven ODI SR loss function \mathcal{L}_{UISR} can be formulated as:

$$\mathcal{L}_{UISR} = \frac{1}{N} \sum_{i=1}^N e^{-s} \left\| I_{HR}^{GT,i} - \mu_{HR}^i \right\|_1 + 2s, \quad (6)$$

where N is the number of pixels, and I_{HR}^{GT} is HR GT image. Except for constraining that the reconstructed high-resolution ODI should be similar to ground truth, \mathcal{L}_{UISR}

Algorithm 1 The overall training process of our framework

- 1: **Training data:** $I_{LR}, I_{HR}^{GT}, D_{LR}^{GT}$
 - 2: **for** for $i=1, i \leq 30$ **do**
 - 3: **ODI SR task:**
 - 4: LR features F_{LR}^{RGB} and F_{LR}^U from I_{LR}
 - 5: Up-sample F_{LR}^{RGB} and F_{LR}^U with CIIFs of parameters g_ρ and g_θ to HR features F_{HR}^{RGB} and F_{HR}^U , respectively
 - 6: SR RGB μ_{HR} and SR uncertainty σ_{HR} from HR features, calculate Eq. (6)
 - 7: **HR depth estimation task:**
 - 8: LR feature F_{LR}^{DE} from I_{LR}
 - 9: LR depth prediction D_{LR} from F_{LR}^{DE} , calculate Eq. (9)
 - 10: **Share CIIF parameters** g_θ
 - 11: Up-sample F_{LR}^{DE} with CIIF of parameters g_θ to HR feature F_{HR}^{DE}
 - 12: HR depth prediction D_{HR} from F_{HR}^{DE} , calculate Eq. (10)
 - 13: **FD loss:**
 - 14: Transform F_{HR}^{RGB} into F_{HR}^T , calculate Eq. (7)
 - 15: HR Transformed depth D_{HR}^T from F_{HR}^T , calculate Eq. (8)
 - 16: **Update framework** with Eq. (11)
 - 17: **end for**
-

additionally emphasizes high-frequency regions that exhibit high uncertainty.

B. Scene Structural Knowledge Transfer (SSKT)

After extracting structural knowledge from the ODI SR task, we propose the SSKT module with two components to transfer the extracted knowledge to the HR depth estimation task, as shown in Fig. 2. Buttressed by the learned interpolation weights of CIIF, we share the parameters g_θ of CIIF between the two tasks. This is because we think the learnable interpolation weights capture the relationships between pixels and thus represent the structural knowledge in both images and depth maps. Besides, to supplement high-resolution detailed features to the HR depth estimation task, we propose the feature distillation (FD) loss to transfer the scene structural knowledge from the ODI SR task, as shown in Fig. 4. The detail of the CIIF sharing strategy and FD loss is introduced in the following part.

CIIF sharing strategy: The CIIF consists of the MLPs and is designed to predict the neural interpolation weights. As the interpolation weights for feature up-sampling can capture the correlations among neighboring pixel features, which can represent the scene structural knowledge. Therefore, it is reasonable to share the parameters g_θ of CIIF between the two tasks for structural knowledge transfer. We do not consider sharing the parameters g_ρ , mainly because it additionally learns textural knowledge that will influence the performance of the HR depth estimation task (See Tab. III). Also, we design to directly share the parameters, instead of asynchronous methods [39] to approximate the parameters of CIIFs. The reason

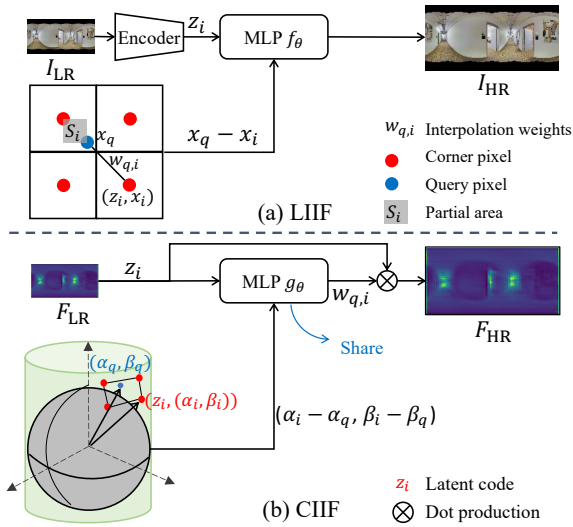


Fig. 3. (a) LIIF predicts the RGB value based on the Cartesian coordinates. (b) Our CIIF learns neural interpolation weights based on the cylindrical coordinates. The parameters of CIIF g_θ are contained in the MLP shared from the ODI SR task.

is that the HR depth estimation task is in a weakly-supervised manner, where the structural details are scarcely possible to be recovered, while the ODI SR task can be fully-supervised to provide rich and fine scene structural details (See Tab. IV). Therefore, directly sharing parameters of CIIF between the two tasks is more effective for structural knowledge transfer.

FD Loss: The CIIF sharing strategy can benefit the feature up-sampling process in the HR depth estimation task. To further enhance the structural details in the HR depth prediction, we propose the FD loss as a structural regularization to help two tasks learn common scene structural knowledge. Although ODIs and their corresponding depth maps are two different representations of the same scene with high geometric similarity, simply applying feature similarity loss, *e.g.*, cosine similarity loss, introduces unnecessary textural knowledge and thus destroys the smoothness of the depth map. As shown in Fig. 4, we first transform the HR feature in the RGB part of the ODI SR network to simulate the HR feature in the HR depth estimation network. Given an HR feature F_{HR}^{RGB} as input, an encoder consisting of three convolutional layers and ReLU activation functions is applied to obtain a transformed feature F_{HR}^T . We then aim to maximize the cosine similarity between F_{HR}^T and HR feature F_{HR}^{DE} from the HR depth estimation network. FD loss can be formulated as follows:

$$\mathcal{L}_{FD} = 1 - \cos(F_{HR}^T, F_{HR}^{DE}). \quad (7)$$

To supervise the transformed feature F_{HR}^T , we cascade a convolutional layer to process F_{HR}^T and output HR transformed depth map D_{HR}^T . Then we down-sample D_{HR}^T with the max-pooling operation M and supervise it using the LR depth GT map D_{LR}^{GT} with Berhu loss \mathcal{B} [40], formulated as follows:

$$\mathcal{L}_T = \mathcal{B}(M(D_{HR}^T) - D_{LR}^{GT}),$$

$$\mathcal{B}(x) = \begin{cases} |x|, & |x| \leq c \\ \frac{x^2 + c^2}{2c}, & |x| > c, \end{cases} \quad (8)$$

where c is a threshold and set to 0.2 empirically [5].

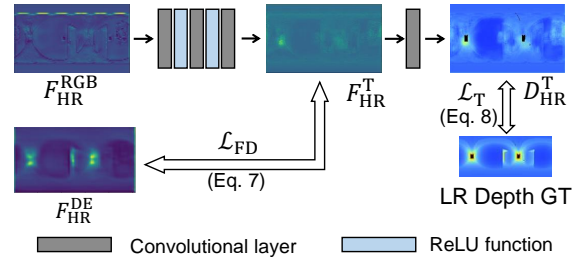


Fig. 4. An illustration of feature distillation (FD) loss.

C. HR Depth Estimation

Lastly, the HR depth estimation network leverages the transferred scene structural knowledge to estimate the HR depth map. As shown in Fig. 2, taking an LR ODI I_{LR} as input, the feature extractor outputs an LR feature F_{LR}^{DE} with the same resolution as I_{LR} . Then, the LR feature I_{LR} is processed with two paths. First, I_{LR} is processed with a convolutional layer to output an LR depth prediction D_{LR} , which is directly supervised by D_{LR}^{GT} through Berhu loss \mathcal{B} as follows:

$$\mathcal{L}_{LD} = \mathcal{B}(D_{LR}, D_{LR}^{GT}). \quad (9)$$

Meanwhile, F_{LR}^{DE} is up-sampled with CIIF of shared parameters g_θ , to generate an HR feature F_{HR}^{DE} . F_{HR}^{DE} is then fed into another convolutional layer to predict an HR depth map D_{HR} . We first down-sample D_{HR} with the max-pooling operation M and then apply Berhu loss to supervise it as follows:

$$\mathcal{L}_{HD} = \mathcal{B}(M(D_{HR}), D_{LR}^{GT}). \quad (10)$$

D. Objective Function

The total loss \mathcal{L}_{TOTAL} includes five parts: uncertainty-driven ODI SR loss \mathcal{L}_{UISR} , FD loss \mathcal{L}_{FD} , and three weakly-supervised depth estimation losses: LR depth estimation loss \mathcal{L}_{LD} , HR depth estimation loss \mathcal{L}_{HD} , and transformed depth estimation loss \mathcal{L}_T . \mathcal{L}_{TOTAL} can be formulated as follows:

$$\mathcal{L}_{TOTAL} = \lambda_1 \mathcal{L}_{UISR} + \lambda_2 \mathcal{L}_{FD} + \lambda_3 \mathcal{L}_{LD} + \lambda_4 \mathcal{L}_{HD} + \lambda_5 \mathcal{L}_T, \quad (11)$$

where $\lambda_i, i \in \{1, 2, 3, 4, 5\}$ is a hyper-parameter for i -th loss term in Eq. (11).

IV. EXPERIMENTS

A. Implementation Details

Dataset. We conduct on three datasets: Stanford2D3D [25], Matterport3D [26] and 3D60 [9]. Stanford2D3D and Matterport3D are real-world datasets, and 3D60 is a synthetic dataset, provided by OmniDepth [9]. We follow UniFuse to split the three datasets respectively. The sizes of ODIs and paired depth maps are 512×1024 in Stanford2D3D and Matterport3D and 256×512 in 3D60. On real-world datasets, the up-sampling factors are set to $\times 4$ and $\times 8$. We train, validate, and test on the two real-world datasets, which are more challenging and have higher resolution than the synthetic dataset. In addition, we test on the synthetic dataset with $\times 8$ up-sampling factor to verify the generalization ability.

TABLE I
 QUANTITATIVE COMPARISON WITH FULLY-SUPERVISED METHODS (WITH HR DEPTH GT) ON STANFORD2D3D AND MATTERPORT3D DATASET.

Dataset	Backbone	Inp. size	Supervision	MAE ↓	Abs Rel ↓	RMSE log ↓	$\delta_1 \uparrow$	$\delta_2 \uparrow$	$\delta_3 \uparrow$
Stanford2D3D [25]	OmniDepth [9]	128×256 (×4)	Fully	0.3248	0.1653	0.1065	77.68	91.71	96.54
			Weakly (Ours)	0.3126	0.1566	0.1043	78.87	92.27	97.03
		64×128 (×8)	Fully	0.3484	0.1830	0.1117	75.71	90.90	96.13
			Weakly (Ours)	0.3480	0.1772	0.1154	75.85	90.59	96.19
	UniFuse-Fusion [5]	128×256 (×4)	Fully	0.2785	0.1409	0.0868	84.01	95.31	98.45
			Weakly (Ours)	0.2784	0.1398	0.0929	82.23	94.20	97.83
		64×128 (×8)	Fully	0.3124	0.1582	0.0975	80.16	93.03	97.46
			Weakly (Ours)	0.3135	0.1585	0.1037	78.06	92.71	97.37
	UniFuse-Equi [5]	128×256 (×4)	Fully	0.2732	0.1403	0.0870	83.70	94.90	98.24
			Weakly (Ours)	0.2747	0.1403	0.0908	83.13	94.83	98.25
		64×128 (×8)	Fully	0.3263	0.1619	0.1011	77.37	92.94	97.33
			Weakly (Ours)	0.3241	0.1630	0.1040	78.69	92.62	97.21
Matterport3D [26]	UniFuse-Fusion [5]	128×256 (×4)	Fully	0.3890	0.1547	0.0966	79.11	92.99	96.97
			Weakly (Ours)	0.3827	0.1569	0.0986	78.75	93.19	97.27
		64×128 (×8)	Fully	0.4779	0.1973	0.1179	70.90	88.98	95.29
			Weakly (Ours)	0.4767	0.2025	0.1220	69.80	89.21	95.57
		256×512 (×4)	Fully	0.3233	0.1314	0.0811	84.39	95.15	98.01
			Weakly (Ours)	0.3152	0.1264	0.0837	85.04	95.30	97.99
	OmniDepth [9]	128×256 (×4)	Fully	0.4483	0.1914	0.1127	72.95	90.21	95.75
			Weakly (Ours)	0.4237	0.1828	0.1082	74.44	91.34	96.51
		64×128 (×8)	Fully	0.4823	0.2127	0.1209	69.80	88.68	95.38
			Weakly (Ours)	0.4843	0.2076	0.1219	69.76	88.70	95.20

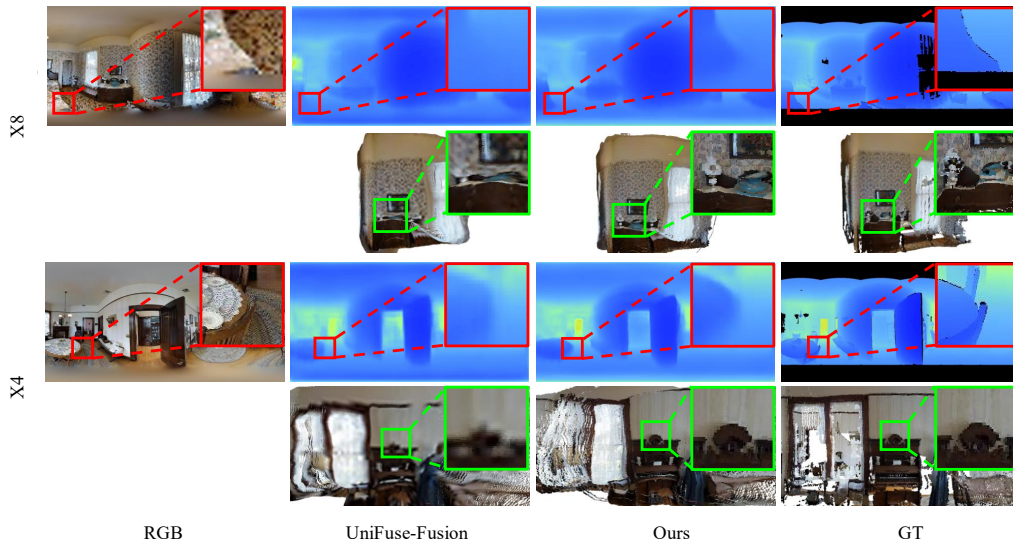


Fig. 5. Visual comparison of fully-supervised method (*i.e.*, UniFuse-Fusion) and ours on Matterport3D dataset. Best viewed in color.

Implementation. We use three omnidirectional depth estimation methods as backbones to extract features from the input ODIs: OmniDepth [9] with spherical convolutions, UniFuse-Fusion [5] with ERP type images and cube maps, and lightweight UniFuse-Equi [5] with only ERP type images. As for the feature extractor of the ODI SR task, we directly employ the commonly-used EDSR-baseline [41] to extract features from the input LR ODIs. We down-sample ODIs with Bicubic interpolation, while down-sample omnidirectional depth maps with Nearest interpolation. During training, we augment data with horizontal flipping and rolling. We collaboratively train the two tasks for 30 epochs using the Adam optimizer [42] with batch size 2. The initial learning rate is set to $1e-4$, and reduced by 2 times per 5 epochs. For hyper-parameters

in \mathcal{L}_{TOTAL} , we empirically set $\lambda_1 = \lambda_2 = 10$, and $\lambda_3 = \lambda_4 = \lambda_5 = 1$. For a fair comparison, we re-train the compared methods based on their provided settings.

B. Quantitative and Qualitative Evaluation

We evaluate our method with standard metrics, including mean absolute error (MAE), absolute relative error (Abs Rel), and root mean square error in log space (RMSE log). We also utilize three accuracy measures (δ_i), which are defined as the fraction of pixels where the relative error between the estimated depth and ground-truth depth is less than the threshold i , $i \in \{1.25, 1.25^2, 1.25^3\}$. We only measure on valid pixels in the ground-truth depth map.

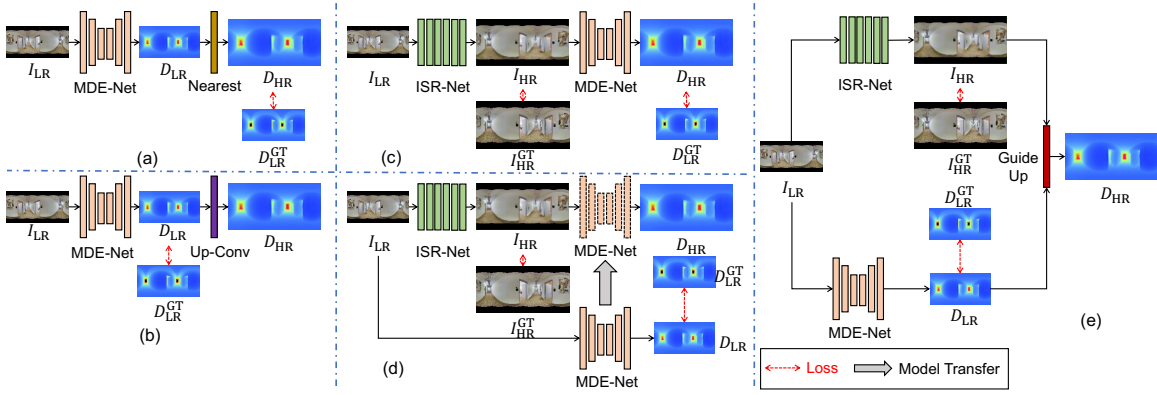


Fig. 6. The pipelines of baseline methods with five different settings. To be consistent with our weakly-supervised setting, these baseline methods only utilize LR ODIs as inputs and LR depth GT maps for supervision. MDE-Net means the monocular depth estimation network, ISR-Net means the ODI super-resolution network, Up-Conv represents the learnable up-sampling convolutional layer, and Guide-Up represents guided image filter [43].

Fully-supervised methods. We compare with fully-supervised methods that utilize HR depth GT maps. To the best of our knowledge, there are no existing methods designed to generate HR depth prediction from an LR ODI. To this end, we add learnable up-sampling convolutional layers to OmniDepth [9], UniFuse-Fusion [5], and UniFuse-Equi [5] and re-train them with HR depth GT maps. As shown in Tab. I, our weakly-supervised method not only achieves comparable results with corresponding fully-supervised methods (*e.g.*, 3rd-4th rows) but also outperforms corresponding supervised methods in some cases (*e.g.*, 1st-2nd rows). For example, in the 4th row of Fig. 5, our method predicts the furniture with regular shapes, while the other corresponding fully-supervised methods predict the shape with more or less warp.

The adaptability of our method in different input sizes is also verified, *e.g.*, 128×256 and 64×128 . Our weakly-supervised method outperforms the fully-supervised methods in several metrics, *e.g.*, MAE, Abs Rel, and δ_3 . For example, with OmniDepth as the backbone with 128×256 input size, our method obtains 3.8% gain in MAE metric and 5.3% gain in Abs Rel metric. When choosing a smaller input size 64×128 , our method has inferior or comparable results compared with the fully-supervised methods. By taking $\times 8$ up-sampling factor and UniFuse-Fusion as the backbone, our method has no metric outperforming the fully supervised method on the Stanford2D3D dataset. We think it is because the LR depth GT map is too sparse, which only contains 1/64 supervision signals of an HR depth GT map.

In addition, we train on the Matterport3D dataset with UniFuse-Fusion and OmniDepth as backbone and achieve comparable results with the corresponding fully-supervised methods. For example, with UniFuse-Fusion as the backbone and $\times 8$ up-sampling factor, our method improves 1.6% in the MAE metric and 0.3% in δ_3 metric. Finally, in Tab. I, we verify the effectiveness of our method with higher resolution, *i.e.*, 1024×2048 . Given the input resolution is 256×512 and the up-sampling factor is 4, the results show that our weakly-supervised method performs well. For example, compared with the fully-supervised method, ours can improve 0.0050 in Abs Rel.

Baseline methods. There are various ways to achieve HR

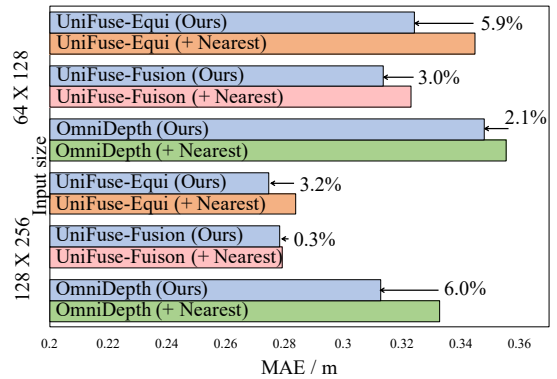


Fig. 7. Quantitative comparison with the baseline methods in the **Setting 1** with different up-sampling factors and backbones on Stanford2D3D dataset.

TABLE II
COMPARISON WITH THE BASELINE METHODS THAT USE LR ODIs AS INPUTS, AND LR DEPTH GROUND TRUTH MAPS FOR SUPERVISION.

	Abs Rel ↓	RMSE log ↓	δ_3 ↑
Setting 2	0.1830	0.1180	95.84
Setting 3	0.3848	0.2847	76.94
Setting 4	0.4523	0.3849	58.17
Setting 5	0.4422	0.2617	78.50
Ours	0.1585	0.1037	97.37

omnidirectional depth estimation using an LR ODI as the input and an LR depth map for supervision. To fully verify the effectiveness of our framework, we compare our method with all possible baseline methods.

1) Setting 1: As shown in Fig. 6(a), it is to estimate LR depth map from LR input ODI, and directly up-sample the LR depth prediction with Nearest interpolation. As shown in Fig. 7, our method outperforms baseline methods with Nearest interpolation in different input sizes and backbones. For example, with OmniDepth as the backbone, our method leads to a 6.0% improvement in the MAE metric, which proves the effects of structural knowledge transfer from the ODI SR task.

2) Setting 2: In Fig. 6(b), it is similar to Setting 1, except for replacing the Nearest interpolation with learnable up-sampling convolutional layers. The result of Setting 2 is 0.1830 Abs Rel metric, which is lower than our method (0.1585 Abs

TABLE III
ABLATION STUDIES ON DIFFERENT SHARING STRATEGIES.

RGB (Mean)	Uncertainty (Variance)	Depth	MAE ↓	Abs Rel ↓
✓	—	✓	0.3225	0.1708
✓		✓	0.3179	0.1588
	✓	✓	0.3135	0.1585
✓	✓	✓	0.3234	0.1686

TABLE IV
ABLATION STUDIES ON CIIF ABOUT WHETHER LEARNING INTERPOLATION WEIGHTS, PARAMETER UPDATE, AND THE TYPE OF COORDINATE SYSTEM.

	Update	Coordinate	MAE ↓	Abs Rel ↓	$\delta_1 \uparrow$
Bicubic	-	-	0.3209	0.1626	77.92
LIIF	Synchronous	Spherical	0.3302	0.1690	76.36
CIIF	Asynchronous	Cylindrical	0.3329	0.1692	76.94
CIIF	Synchronous	Cylindrical	0.3135	0.1585	78.06

Rel). We analyze the reason that the additional up-sampling convolutional layer can not be fully supervised by HR depth GT maps, causing its performance to drop greatly.

3) Setting 3: In Fig. 6(c), it is to first up-sample LR ODIs with an ODI SR network, *i.e.*, EDSR-baseline [41], which is fully-supervised with HR ground truth ODIs. Then, the super-resolved ODI is fed into a depth estimation network to generate an HR depth prediction. The HR depth prediction is down-sampled with the Nearest interpolation to be compared with the LR depth GT map. In Tab. II, setting 3 performs badly, due to the super-resolved ODI containing much noise, which disturbs the following depth estimation network.

4) Setting 4: In Fig. 6(d), it is similar to Setting 3, except that the depth estimation network is trained with LR ODI as input. We then directly transfer the pre-trained depth estimation network into the HR domain with the super-resolved ODI as input. However, it only obtains 0.4523 Abs Rel, which is worse than Setting 3 and our method. Its main drawback is that during training, the depth estimation network has no access to HR ODIs or HR depth maps.

5) Setting 5: In Fig. 6(e), it first predicts a super-resolved image with an ODI SR network, *i.e.*, EDSR-baseline [41], and an LR depth prediction with a depth estimation network. Then, it utilizes the super-resolved ODI to guide the interpolation process of the LR depth prediction with guided image filter [43]. However, the result is similar to that of Setting 4, due to the noise contained in the super-resolved image.

C. Ablation Studies

We conduct on the Stanford2D3D dataset with $\times 8$ factor.

Uncertainty estimation. In the first row of Tab. III, we first omit uncertainty estimation in the ODI SR task and share the parameters of CIIF between feature up-sampling processes in the ODI SR task and HR depth estimation task. Removing uncertainty estimation leads to 2.8% MAE and 7.2% Abs Rel reduction. Directly transferring knowledge between the ODI SR task and the HR depth estimation task obtains sub-optimal performance, because the redundant textural details in the ODI SR task might interfere with the HR depth estimation task.

Sharing strategy of CIIF. To verify the effectiveness of our proposed sharing strategy, we additionally experiment on other

TABLE V
ABLATION STUDIES ON LOSS FUNCTIONS.

\mathcal{L}_{LD}	\mathcal{L}_{FD}	Transform	Abs Rel ↓	$\delta_3 \uparrow$
	✓	✓	0.1642	97.30
✓			0.1655	97.10
✓	✓		0.1723	97.34
✓	✓	✓	0.1585	97.37

TABLE VI
COMPARISON OF ESTIMATING UNCERTAINTY (OURS) WITH ESTIMATING THE GRADIENT FOR THE ODI SR TASK.

	MAE ↓	Abs Rel ↓	$\delta_1 \uparrow$
Gradient	0.3141	0.1635	78.30
Uncertainty (Ours)	0.3135	0.1585	78.06

combinations in Tab. III. Specifically, in the second row, we choose to share the parameters of CIIF between feature up-sampling processes in the RGB part of the ODI SR task, and the HR depth estimation task. Moreover, we study the influence of sharing the parameters among the feature up-sampling processes in the RGB part of the ODI SR task, the uncertainty part of the ODI SR task, and the HR depth estimation task. However, we find that Abs Rel degrades 6.0% compared with sharing between the uncertainty part and HR depth estimation task. It also proves that textural details of directly transferring knowledge from features in the RGB part of the ODI SR task can cause negative effects on the structural knowledge learning of the HR depth estimation task.

Components of CIIF. We replace CIIF with Bicubic interpolation followed by a convolution layer, which is commonly used in [5], [8]. In Tab. IV, we find that CIIF gains 2.5% in Abs Rel. We ascribe it as learning correlation among adjacent pixels is more effective for structural knowledge learning and transferring between different modals.

The parameters of CIIF are all contained in an MLP. We share the parameters of CIIF between the ODI SR task and the HR depth estimation task. To verify it, we conduct a momentum update [39] for the HR depth estimation task, which is considered as an asynchronous update. From Tab. IV, asynchronous update reduces performance greatly. We think the reason is that scene structural knowledge is essential for the HR depth estimation task, and asynchronous update destroys the common structural representations between the two tasks.

In addition, we investigate the effectiveness of cylindrical representation. As shown in Tab. IV, exploiting cylindrical representation obtains a 5.1% gain in MAE metric compared with utilizing spherical angle coordinates. Note that using spherical angle coordinates is equal to using planar pixel coordinates in LIIF [3], [31]. The result demonstrates that the cylindrical coordinate system is more proper to describe the spatial correlation of neighboring pixels in ERP type ODIs.

Loss function. By default, \mathcal{L}_{UISR} and \mathcal{L}_{HD} are necessary for the training. Therefore, we investigate the effectiveness of \mathcal{L}_{LD} and \mathcal{L}_{FD} . In Tab. V, without \mathcal{L}_{LD} , the performance degrades 3.5% in Abs Rel metric. It demonstrates that \mathcal{L}_{LD} can utilize the LR depth GT maps to help obtain more accurate LR features for the HR depth estimation task. Without \mathcal{L}_{FD} , the performance also degrades 1.6% in the RMSE log metric.

TABLE VII
DISCUSSION ABOUT EMPLOYING DIFFERENT BACKBONES FOR THE ODI SR TASK.

	Abs Rel ↓	δ_3 ↑
SwinIR [45]	0.1673	96.99
Omni-SR [46]	0.1733	96.86
EDSR-baseline [41]	0.1585	97.37

TABLE VIII
COMPARISON OF GENERALIZATION CAPABILITY.

	Method	MAE ↓	δ_3 ↑
Stanford2D3D →3D60	UniFuse-Fusion [5]	0.4816	94.51
	Ours	0.4637	95.02
Matterport3D →3D60	UniFuse-Fusion [5]	0.3974	96.88
	Ours	0.3629	97.05
Stanford2D3D →3D60	OmniDepth [9]	0.9735	71.07
	Ours	0.7761	81.47
Matterport3D →3D60	OmniDepth [9]	0.4363	95.29
	Ours	0.4250	95.95

In addition, we omit the transformation process and find that the Abs Rel metric degrades from 0.1585 to 0.1723.

D. Discussion

Structural representation. To investigate the form of structural representation, we replace uncertainty estimation with gradient estimation [44]. In Tab. VI, uncertainty estimation performs better than gradient estimation. Compared with the gradient that only matches fixed edges of ODIs with the certain data distribution [24], uncertainty estimation is from the data itself and is more flexible for learning structural knowledge.

Different ODI SR backbones. In Tab. VII, we compare the performance with different backbones in the ODI SR task. *i.e.*, SwinIR, Omni-SR, and EDSR-baseline. However, we find that by employing deeper SR backbones, the performance of depth estimation drops. We think the reason is that the deeper SR backbones are not easy to train. Specifically, the Stanford2D3D dataset only contains 1000 training samples, which is not friendly for attention-based backbones.

Generalization ability. To verify it, we further test on 3D60 dataset with pre-trained depth estimation models, *i.e.*, OmniDepth and UniFuse-Fusion, from Stanford2D3D and Matterport3D datasets in Tab. VIII. With UniFuse-Fusion as the backbone, our weakly-supervised method outperforms the corresponding fully-supervised method, *e.g.*, 3.7% gain and 8.7% gain in MAE metric on Stanford2D3D dataset and Matterport3D dataset, respectively. With OmniDepth as the backbone, our method also shows significant improvements, *e.g.*, 10.40% and 0.66% in δ_3 metric on Stanford2D3D and Matterport3D datasets, respectively.

V. CONCLUSION

In this paper, to the best of our knowledge, we proposed the first work to estimate the HR omnidirectional depth map directly from an LR ODI, when no HR depth GT map is available. We found that the ODIs and paired depth maps share the common scene structural knowledge. Therefore, we introduced an ODI SR task to boost the performance of the HR depth

estimation task. Especially, the textural details in the ODI SR task can interfere with the smoothness of depth predictions. In this case, we introduced uncertainty estimation to the ODI SR specially for extracting scene structural knowledge. Upon this, we proposed the CIIF and FD loss in the SSKT module. The CIIF captures the correlations among neighboring pixels and shares the scene structural knowledge between the two tasks, while the FD loss provides extra structural regularization. Experimental results demonstrated that our weakly-supervised method is 1) efficient without extra inference cost, 2) flexible as a plug-and-play approach, and 3) effective in achieving comparable results with the fully-supervised methods.

Limitation and future work: In this paper, we achieve the high-resolution 360° depth estimation task via weakly-supervised learning. In this way, we alleviate the difficulty of acquiring high-resolution 360° depth ground truth. However, acquiring a 360° depth map is inherently difficult due to stitching and alignment processes. Recently, the depth foundation models of perspective depth estimation have risen by exploiting large-scale labeled and unlabeled perspective images [47]. In the future, we plan to excavate knowledge from such rich perspective images and depth maps, which is an appealing direction to inspire the 360° depth estimation.

APPENDIX

Abstract—We provide more details of the proposed method in the supplementary material. Specifically, in Sec. A we explain explicitly the proposed cylindrical implicit interpolation function (CIIF) and its sharing strategy. Sec. B shows more details in the feature distillation (FD) loss. Then, Sec. C shows the more experimental results, including datasets and metrics, visual comparisons, ablation studies, and reports on inference time.

A. Cylindrical Implicit Interpolation Function

1) *Implicit Image Function*: In general, the image interpolation problem can be defined as follows:

$$I_{hr}(x_q) = \sum_{i \in N_q} w_{q,i} v_{q,i}, \quad (12)$$

as shown in Fig. 9(a), where x_q is the coordinate of query pixel q in the HR image domain, x_i is the coordinate of corner pixel $i \in \{00, 01, 10, 11\}$ in the LR image domain and N_q is the set of neighbor pixels for q , $w_{q,i}$ is the interpolation weight between q and i , and $v_{q,i}$ is the interpolation value. $I_{hr}(x_q)$ is the pixel value of q . In traditional image interpolation, the pixel value $I_{lr}(x_i)$ is commonly used as the interpolation value $v_{q,i}$. Due to the nature of perspective images, N_q is usually chosen as the four nearest corner pixels of q in the LR domain (as illustrated in Fig. 9(a), $i \in \{00, 01, 10, 11\}$), and the interpolation weight $w_{q,i}$ is often chosen as the partial area diagonally opposite the corner pixel i (e.g., in Fig. 9(a), interpolation weight $w_{q,00} = S_{00}$), such as Bilinear interpolation.

In implicit image function [32], [48], the image coordinates are normalized into $(-1, 1)$ to make it possible to share the coordinate in the LR image domain and the HR image domain. In this way, [32], [48] can achieve arbitrary up-sampling factors by querying the pixels in the HR image domain according to corresponding coordinates. For example in Fig. 9(a), we can follow the coordinate $(-0.5, -0.5)$ to query the pixel x_{00} in the LR image domain and follow the coordinate $(-0.125, -0.125)$ to query the pixel x_q in the HR image domain.

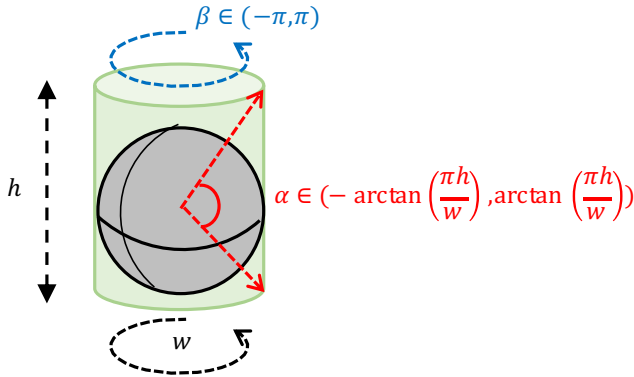


Fig. 8. The illustration of cylinder angle coordinate system for ERP images.

Furthermore, as shown in Fig. 9(b), in implicit image functions, instead of directly using the pixel value (e.g., RGB

value and depth value), the interpolation value $v_{q,i}$ is often generated through a multi-layer perceptron (MLP) g_θ which takes the latent code z_i from an image feature extractor and the relative coordinate $x_q - x_i$ as input, formulated as:

$$v_{q,i} = g_\theta(z_i, x_q - x_i). \quad (13)$$

In IJIF [32], as shown in Fig. 9(c), instead of utilizing the partial area, the interpolation weight $w_{q,i}$ is predicted together with the interpolation value $v_{q,i}$ through an MLP, which views the interpolation weight and the interpolation value as the edge and the node in a graph model, and can be written as:

$$w_{q,i}, v_{q,i} = g_\theta(z_i, x_q - x_i). \quad (14)$$

2) *Cylindrical Representation*: The aforementioned implicit image functions are designed for perspective images based on Cartesian coordinate system, which are not applicable for omnidirectional images. This is because omnidirectional images are from a sphere, and the most popular equirectangular projection (ERP) is unfold from the sphere based on Cylindrical coordinate system. Using Cartesian coordinate system makes the left side and right side of an ERP image not contiguous. To better represent the spatial correlation of pixels in ERP images, we reframe ERP images with cylindrical representation, as shown in Fig. 8. Note that the range of the cylindrical angle coordinate system (α, β) is:

$$\alpha \in (-\arctan(\frac{\pi h}{w}), \arctan(\frac{\pi h}{w})), \quad (15)$$

$$\beta \in (-\pi, \pi).$$

In this case, our CIIF can be formulated as $g_\theta(z_i, (\alpha_i - \alpha_q, \beta_i - \beta_q))$. As for the output content, we will discuss it in Sec. A3 according to our specific framework and demand.

3) *Sharing Strategy*: In the above discussion, we have reframed CIIF in cylindrical representation. The aim of CIIF is to transfer structural knowledge from the ODI SR task to the HR depth estimation task. The ODIs and their corresponding depth maps are two different representations for the same scene, which implies that both modals contain the common structural knowledge. Therefore, we directly choose to share parameters of CIIF between the ODI SR task and HR depth estimation task. Note that the parameters of CIIF are all included in an MLP.

As for the output form of CIIF, we find that the predicted interpolation value $v_{q,i}$ in Eq. 13 and Eq. 14 can not be shared between different modals. Instead, the relative correlation among neighboring pixels can effectively represent the common structural knowledge of the same scene, depicted as the interpolation weight $w_{q,i}$. In this case, we only output the interpolation weights $w_{q,i}$ from an MLP, formulated as follows:

$$w_{q,i} = g_\theta(z_i, (\alpha_i - \alpha_q, \beta_i - \beta_q)). \quad (16)$$

4) *Feature Up-sampling Process*: As shown in Fig. 10, given an LR feature map $F_{lr} \in h \times w \times c$, we aim to obtain an HR feature map $F_{hr} \in sh \times sw \times c$, where s is the up-sampling factor. An MLP with hidden dimension

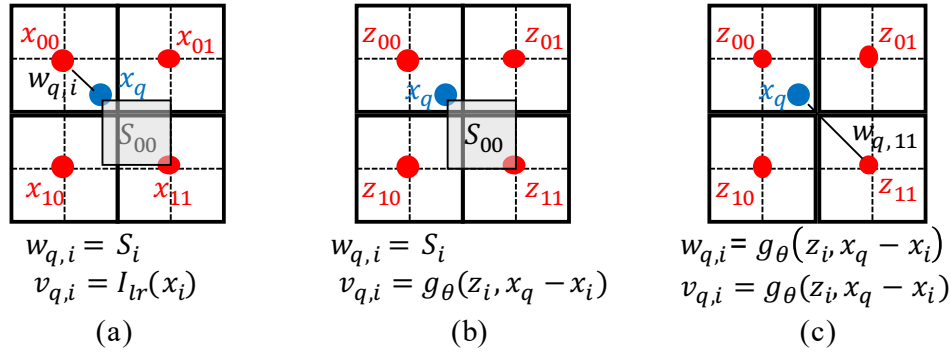


Fig. 9. (a) General image interpolation process. (b) LIIF [48]. (c) JIIF [32].

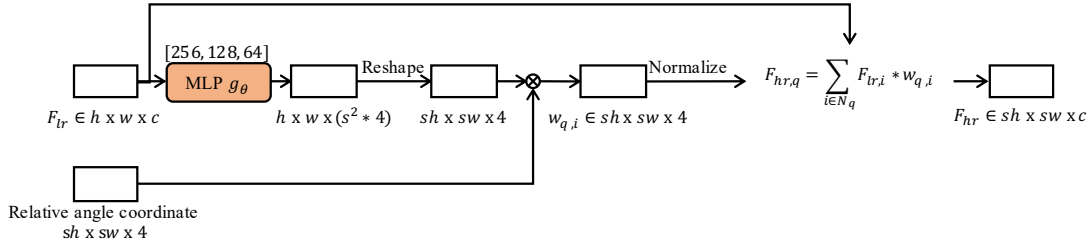


Fig. 10. The illustration of the up-sampling process from LR feature to HR feature with our CIIF.

TABLE IX
THE NUMBER OF SAMPLES IN TRAINING SET, VALIDATION SET, AND TESTING SET IN THREE DATASETS.

	Dataset		
	Stanford2D3D [25]	Matterport3D [26]	3D60 [9]
Training	1000	7829	–
Validation	40	947	–
Testing	373	2014	1298

[256, 128, 64] is employed to output interpolation weights $w_{q,i} \in h \times w \times (4 * s^2)$. Then, interpolation weights $w_{q,i}$ is reshaped to $sh \times sw \times 4$. We add in the cylindrical relative angle coordinate with the form $\cos(\alpha_i - \alpha_q) * \cos(\beta_i - \beta_q)$. We normalize $w_{q,i}$ in the third dimension by $w_{q,i} = \frac{w_{q,i}}{\sum_{i \in \mathcal{N}_q} w_{q,i}}$, and thus each query pixel q in the HR domain has four normalized interpolation weights associated with four corner pixels. Then, F_{hr} is obtained with $w_{q,i}$ and F_{lr} based on Eq. 12, where F_{lr} is the interpolation values.

B. FD Loss

We visualize the HR ODI, the HR RGB feature from the ODI SR task, the HR transformed feature and the HR feature from the HR depth estimation task in Fig. 11, respectively. We can find that before transformation, the HR RGB feature from the ODI SR task contains much texture information, which interferes with the smoothness of the HR depth estimation. Instead, the HR transformed feature is more similar with the HR feature from the HR depth estimation task, which is more appropriate for matching the similarity between different tasks.

C. Experiment

1) **Dataset and Metrics: Dataset.** We follow the split files of UniFuse³ to split the three datasets respectively, as depicted in Tab. IX. As the 3D60 dataset is only used to verify the generalization ability, the splits of its training and validation subsets are omitted.

Metrics. We evaluate our method with standard metrics introduced in [5]. We only calculate the observed pixels $p \in \text{obs}$, which are valid in the HR depth GT maps D_{HR}^{GT} . Notably, during training, our weakly-supervised method only utilizes LR depth maps D_{LR}^{GT} as the supervision, while HR depth GT maps D_{HR}^{GT} is only utilized for evaluation. Given D_{HR}^{GT} and HR depth prediction D_{HR} , the metrics include:

- Mean Absolute Error (MAE) measures the absolute difference between the depth prediction and ground truth. It is to show how close between the prediction and ground truth.

$$\frac{1}{N_{\text{obs}}} \sum_{p \in \text{obs}} \|D_{HR}(p) - D_{HR}^{GT}(p)\|. \quad (17)$$

- Absolute Relative Error (Abs Rel) measures the absolute difference between the depth prediction and ground truth, scaled by the ground truth. It is to express how large the error is compared with the ground truth.

$$\frac{1}{N_{\text{obs}}} \sum_{p \in \text{obs}} \frac{\|D_{HR}(p) - D_{HR}^{GT}(p)\|}{D_{HR}^{GT}(p)}. \quad (18)$$

- Root Mean Square Error in log space (RMSE log) measures the square root of the squared difference. The squared difference can emphasize the scenes with large

³<https://github.com/alibaba/UniFuse-Unidirectional-Fusion/tree/main/UniFuse/datasets>

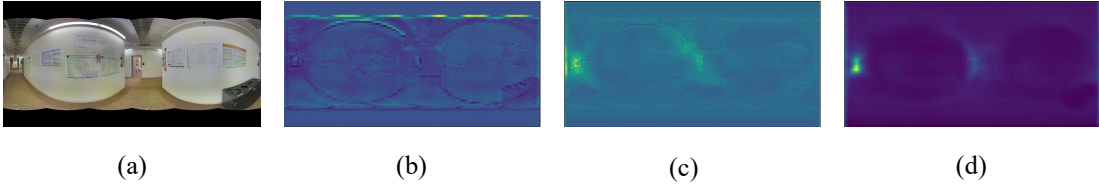


Fig. 11. Visualization of the features employed in the FD loss. (a) HR ODI. (b) HR RGB feature from the ODI SR task. (c) HR transformed feature. (d) HR feature from the HR depth estimation task.

TABLE X
ABLATION STUDIES ON BERHU LOSS.

	Abs Rel ↓	δ_3 ↑
L1 loss	0.1609	97.18
Berhu loss [40]	0.1585	97.37

TABLE XI
ABLATION STUDIES ON THE EFFECT OF SPHERICAL CONVOLUTIONS.

EquiConv	MAE ↓	Abs Rel ↓	δ_1 ↑
✓	0.3144	0.1589	79.16
	0.3135	0.1585	78.06

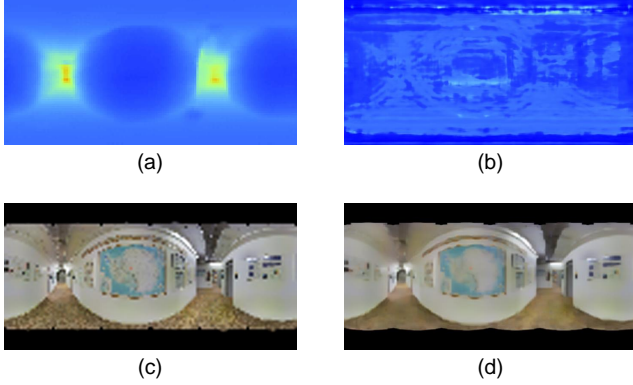


Fig. 12. Illustration of the “noise problem”. (a) The predicted HR depth map in Setting 1; (b) the predicted HR depth map in Setting 3; (c) the LR input in Setting 1; (d) the super-resolved ODI in Setting 3.

depth variances. In addition, utilizing the log form can emphasize scale differences instead of absolute distance differences.

$$\sqrt{\frac{1}{N_{\text{obs}}} \sum_{p \in \text{obs}} \|\log_{10} D_{\text{HR}}(p) - \log_{10} D_{\text{HR}}^{\text{GT}}(p)\|^2}. \quad (19)$$

- δ_i , the fraction of pixels where the relative error between the depth prediction D_{HR} and depth GT map $D_{\text{HR}}^{\text{GT}}$ is less than the threshold 1.25^i , $i \in \{1, 2, 3\}$. It is to evaluate the accuracy ratios rather than absolute or squared differences.

$$\max\left\{\frac{D_{\text{HR}}(p)}{D_{\text{HR}}^{\text{GT}}(p)}, \frac{D_{\text{HR}}^{\text{GT}}(p)}{D_{\text{HR}}(p)}\right\} < i, \quad (20)$$

where N_{obs} represents the total number of the observed pixels in $D_{\text{HR}}^{\text{GT}}$.

2) *Ablation Studies: Berhu loss.* In Tab. X, it can be seen that employing Berhu loss [40] has an improvement in both metrics, such as 0.0024 in Abs Rel metric, which can benefit the depth estimation performance.

TABLE XII
INVESTIGATION OF APPLYING CIIF TO THE FULLY-SUPERVISED METHODS.

	MAE ↓	Abs Rel ↓	δ_1 ↑
Conv	0.3124	0.1582	80.16
CIIF	0.3049	0.1577	79.66

TABLE XIII
ABLATION STUDIES ON FD LOSS ABOUT DIFFERENT CALCULATIONS OF FEATURE SIMILARITY AND WHETHER APPLYING TRANSFORM.

	Transform	Abs Rel ↓	δ_3 ↑
Feature affinity [37]		0.1645	96.93
	✓	0.1630	97.42
Cosine similarity		0.1723	97.34
	✓	0.1585	97.37

Spherical convolutions. Recently, some efforts have been made to adjust the shape [9] and sampling location [11] of convolution filters to address the distortion problem in ERP type ODI. To verify if the spherical convolution benefits our framework, we choose EquiConvs, which is characterized by their irregular convolutional kernels to adapt to the varying distortions across different latitudes. However, as introduced in BiFuse [7], the effectiveness of EquiConvs is uncertain, especially in deeper networks. As shown in Table XI, the results show that the influence caused by EquiConvs is minor (0.0009 drop in MAE, and 1.10% improvement in δ_1). Therefore, it is reasonable that our design in knowledge transfer is more important than applying the EquiConvs.

FD loss. We further investigate the choice of different calculations of feature similarity in Tab. XIII. Without transform, the feature affinity loss [37] even performs worse than cosine-similarity. After adding the transform process, the feature affinity loss improves in both metrics, such as 0.49% in δ_3 metric. The results show that the transform process is more important than the selection of the calculation of feature similarity.

3) *Discussion: Adding CIIF to current methods.* In the main paper, the fully-supervised methods are learnable up-sampling convolutional layers, such as combining Bicubic up-sampling and convolution layers, which is used in UniFuse. In Tab. XII, we try to replace the learnable up-sampling layers with our CIIF. We find that the performance of the fully-supervised can be improved significantly, such as 0.0075 in MAE metric. It demonstrates the effectiveness of the CIIF.

Different ODI SR backbones. In Setting 3 and 5, the choice of deeper SR backbones might provide more accurate SR ODI for the followed depth estimation network. However, In Tab. XIV, we find that the depth estimation results in Setting

TABLE XIV

DISCUSSION ABOUT THE EFFECT OF EMPLOYING SWINIR, WHICH IS A DEEPER SR BACKBONE.

Setting	Abs Rel ↓	RMSE log ↓	δ_3 ↑
3	0.3414	0.2630	75.25
5	0.4717	0.2653	77.73

TABLE XV

COMPARISON OF COMPUTATIONAL COSTS AND TIME CONSUMING FOR FEATURE UP-SAMPLING BETWEEN BICUBIC INTERPOLATION AND OUR CIIF.

	CIIF	Bicubic
GFLOPs	0.65	1.21
Time (ms)	26.5	0.5

TABLE XVI

COMPARISON OF COMPUTATIONAL COSTS AMONG DIFFERENT INPUT SIZES AND OUTPUT SIZES.

Depth Backbone	Input Size	Output Size	GFLOPs
OmniDepth [9]	128 × 256	512 × 1024	21
	512 × 1024		317
	256 × 512	1024 × 2048	86
	1024 × 2048		1267
UniFuse-Fusion [5]	128 × 256	512 × 1024	6
	512 × 1024		63
	256 × 512	1024 × 2048	22
	1024 × 2048		250

3 and 5 are still bad. To better illustrate the noise problem, we provide the visualization results in Fig. 12. We observe that the predicted HR depth map from the LR ODI in Setting 1 is obviously better than the predicted result from the SR ODI in Setting 3. In contrast, our framework do not utilize the SR image, but utilize the SR features for knowledge distillation.

Computational costs and inference time. We further report the computational costs with different input sizes and output sizes in Tab. XVI. With OmniDepth as backbone, to achieve the goal of HR depth estimation with 1024 × 2048, our method needs 86 GFLOPs. However, with the input of the original resolution, the computational costs increase to 1267 GFLOPs, which is about 15 times of our method. It demonstrates that our method relieves the computational burden with LR ODI as input during inference.

As shown in Fig. 13, we calculate computational costs with ×8 up-sampling factor, EDSR-baseline [41] as the feature extractor in the ODI SR task, and UniFuse-Fusion [5] as the feature extractor in the HR depth estimation task. During training, the feature extractor in the ODI SR task has 9.829 GFLOPs, and the feature extractor in the HR depth estimation task has 0.977 GFLOPs. CIIF which serves for up-sampling feature maps consumes 0.654 GFLOPs. The decoder of each modal is also reported. Once training is done, the ODI SR task can be freely removed, introducing no extra inference cost. Therefore, the overall inference cost is only 1.706 GFLOPs.

4) *More visual results.*: In Fig. 13, we provide more visual results on Matterport3D dataset. In addition, in Fig. 15, we provide visual comparisons about ablation studies.

REFERENCES

- [1] E. Galván and P. Mooney, “Neuroevolution in deep neural networks: Current trends and future challenges,” *IEEE Transactions on Artificial Intelligence*, vol. 2, no. 6, pp. 476–493, 2021.
- [2] D. Eigen, C. Puhrsch, and R. Fergus, “Depth map prediction from a single image using a multi-scale deep network,” in *NIPS*, 2014.
- [3] H. Ai, Z. Cao, J. Zhu, H. Bai, Y. Chen, and L. Wang, “Deep learning for omnidirectional vision: A survey and new perspectives,” *arXiv preprint arXiv:2205.10468*, 2022.
- [4] C. Sun, M. Sun, and H.-T. Chen, “Hohonet: 360 indoor holistic understanding with latent horizontal features,” in *CVPR*, 2021, pp. 2573–2582.
- [5] H. Jiang, Z. Sheng, S. Zhu, Z. Dong, and R. Huang, “Unifuse: Unidirectional fusion for 360° panorama depth estimation,” *IEEE Robotics and Automation Letters*, vol. 6, pp. 1519–1526, 2021.
- [6] H. Ai, Z. Cao, Y. pei Cao, Y. Shan, and L. Wang, “Hrdfuse: Monocular 360° depth estimation by collaboratively learning holistic-with-regional depth distributions,” *ArXiv*, vol. abs/2303.11616, 2023.
- [7] F.-E. Wang, Y. hsuan Yeh, M. Sun, W.-C. Chiu, and Y.-H. Tsai, “Bifuse: Monocular 360 depth estimation via bi-projection fusion,” *CVPR*, pp. 459–468, 2020.
- [8] Y. Li, Y. Guo, Z. Yan, X. Huang, Y. Duan, and L. Ren, “Omnifusion: 360 monocular depth estimation via geometry-aware fusion,” in *CVPR*, 2022, pp. 2801–2810.
- [9] N. Zioulis, A. Karakottas, D. Zarpalas, and P. Daras, “OmniDepth: Dense depth estimation for indoors spherical panoramas,” in *ECCV*, 2018.
- [10] M. Rey-Area, M. Yuan, and C. Richardt, “360monodepth: High-resolution 360° monocular depth estimation,” *CVPR*, pp. 3752–3762, 2022.
- [11] K. Tateno, N. Navab, and F. Tombari, “Distortion-aware convolutional filters for dense prediction in panoramic images,” in *ECCV*, 2018.
- [12] C. Zhuang, Z. Lu, Y. Wang, J. Xiao, and Y. Wang, “Acndnet: Adaptively combined dilated convolution for monocular panorama depth estimation,” *arXiv preprint arXiv:2112.14440*, 2021.
- [13] C.-H. Peng and J. Zhang, “High-resolution depth estimation for 360deg panoramas through perspective and panoramic depth images registration,” in *Proceedings of the IEEE/CVF Winter Conference on Applications of Computer Vision*, 2023, pp. 3116–3125.
- [14] S. Mangiante, G. Klas, A. Navon, Z. GuanHua, J. Ran, and M. D. Silva, “Vr is on the edge: How to deliver 360 videos in mobile networks,” in *Proceedings of the Workshop on Virtual Reality and Augmented Reality Network*, 2017, pp. 30–35.
- [15] B. Sun, X. Ye, B. Li, H. Li, Z. Wang, and R. Xu, “Learning scene structure guidance via cross-task knowledge transfer for single depth super-resolution,” *2021 IEEE/CVF Conference on Computer Vision and Pattern Recognition (CVPR)*, pp. 7788–7797, 2021.
- [16] A. Geiger, P. Lenz, and R. Urtasun, “Are we ready for autonomous driving? the kitti vision benchmark suite,” in *2012 IEEE conference on computer vision and pattern recognition*. IEEE, 2012, pp. 3354–3361.
- [17] Y. Li and J. Ibanez-Guzman, “Lidar for autonomous driving: The principles, challenges, and trends for automotive lidar and perception systems,” *IEEE Signal Processing Magazine*, vol. 37, no. 4, pp. 50–61, 2020.
- [18] X. Deng, H. Wang, M. Xu, Y. Guo, Y. Song, and L. Yang, “Lau-net: Latitude adaptive upscaling network for omnidirectional image super-resolution,” *CVPR*, pp. 9185–9194, 2021.
- [19] Y.-S. Yoon, I. Chung, L. Wang, and K.-J. Yoon, “Spheresr: 360° image super-resolution with arbitrary projection via continuous spherical image representation,” *ArXiv*, vol. abs/2112.06536, 2021.
- [20] M. Zhang, Q. Wu, J. Guo, Y. Li, and X. Gao, “Heat transfer-inspired network for image super-resolution reconstruction,” *IEEE Transactions on neural networks and learning systems*, 2022.
- [21] M. Zhang, J. Xin, J. Zhang, D. Tao, and X. Gao, “Curvature consistent network for microscope chip image super-resolution,” *IEEE Transactions on Neural Networks and Learning Systems*, 2022.
- [22] M. Zhang, Q. Wu, J. Zhang, X. Gao, J. Guo, and D. Tao, “Fluid micelle network for image super-resolution reconstruction,” *IEEE Transactions on Cybernetics*, vol. 53, no. 1, pp. 578–591, 2022.
- [23] K. Karsch, C. Liu, and S. B. Kang, “Depth transfer: Depth extraction from video using non-parametric sampling,” *IEEE transactions on pattern analysis and machine intelligence*, vol. 36, no. 11, pp. 2144–2158, 2014.
- [24] Q. Ning, W. Dong, X. Li, J. Wu, and G. Shi, “Uncertainty-driven loss for single image super-resolution,” *Advances in Neural Information Processing Systems*, vol. 34, 2021.
- [25] I. Armeni, S. Sax, A. R. Zamir, and S. Savarese, “Joint 2d-3d-semantic data for indoor scene understanding,” *ArXiv*, vol. abs/1702.01105, 2017.

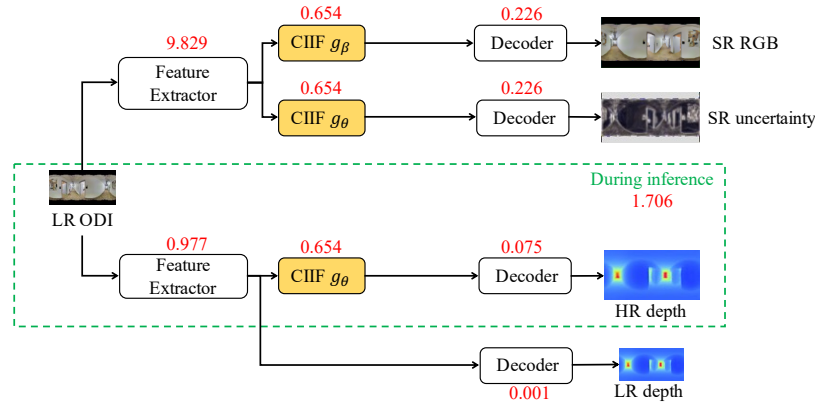


Fig. 13. Overview of computational costs of each module.

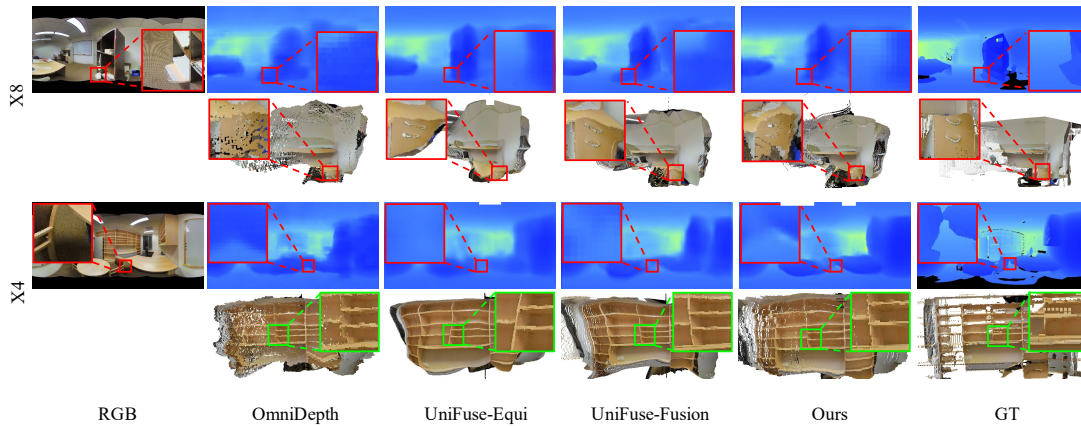


Fig. 14. Visual comparison of fully-supervised methods and ours on Stanford2D3D dataset. Best viewed in color.

- [26] A. Chang, A. Dai, T. Funkhouser, M. Halber, M. Niessner, M. Savva, S. Song, A. Zeng, and Y. Zhang, "Matterport3d: Learning from rgb-d data in indoor environments," *arXiv preprint arXiv:1709.06158*, 2017.
- [27] Z. Shen, C. Lin, K. Liao, L. Nie, Z. Zheng, and Y. Zhao, "Panoformer: Panorama transformer for indoor 360 depth estimation," *arXiv e-prints*, pp. arXiv-2203, 2022.
- [28] M. Li, S. Wang, W. Yuan, W. Shen, Z. Sheng, and Z. Dong, "S2net: Accurate panorama depth estimation on spherical surface," *IEEE Robotics and Automation Letters*, vol. 8, no. 2, pp. 1053–1060, 2023.
- [29] C. Ozcinar, A. Rana, and A. Smolic, "Super-resolution of omnidirectional images using adversarial learning," *2019 IEEE 21st International Workshop on Multimedia Signal Processing (MMSp)*, pp. 1–6, 2019.
- [30] K.-S. Chung and C. Lee, "Gram: Gradient rescaling attention model for data uncertainty estimation in single image super resolution," *2019 18th IEEE International Conference On Machine Learning And Applications (ICMLA)*, pp. 8–13, 2019.
- [31] Y. Chen, S. Liu, and X. Wang, "Learning continuous image representation with local implicit image function," in *CVPR*, 2021, pp. 8628–8638.
- [32] J. Tang, X. Chen, and G. Zeng, "Joint implicit image function for guided depth super-resolution," in *Proceedings of the 29th ACM International Conference on Multimedia*, 2021, pp. 4390–4399.
- [33] S. Niu, Y. Liu, J. Wang, and H. Song, "A decade survey of transfer learning (2010–2020)," *IEEE Transactions on Artificial Intelligence*, vol. 1, no. 2, pp. 151–166, 2020.
- [34] M. Zhang, R. Wang, X. Gao, J. Li, and D. Tao, "Dual-transfer face sketch-photo synthesis," *IEEE Transactions on Image Processing*, vol. 28, no. 2, pp. 642–657, 2018.
- [35] M. Zhang, N. Wang, Y. Li, and X. Gao, "Deep latent low-rank representation for face sketch synthesis," *IEEE transactions on neural networks and learning systems*, vol. 30, no. 10, pp. 3109–3123, 2019.
- [36] —, "Neural probabilistic graphical model for face sketch synthesis," *IEEE transactions on neural networks and learning systems*, vol. 31, no. 7, pp. 2623–2637, 2019.
- [37] L. xilinx Wang, D. Li, Y. Zhu, L. Tian, and Y. Shan, "Dual super-resolution learning for semantic segmentation," *2020 IEEE/CVF Conference on Computer Vision and Pattern Recognition (CVPR)*, pp. 3773–3782, 2020.
- [38] D.-A. Clevert, T. Unterthiner, and S. Hochreiter, "Fast and accurate deep network learning by exponential linear units (elus)," *arXiv: Learning*, 2015.
- [39] K. He, H. Fan, Y. Wu, S. Xie, and R. Girshick, "Momentum contrast for unsupervised visual representation learning," in *CVPR*, 2020, pp. 9729–9738.
- [40] I. Laina, C. Rupprecht, V. Belagiannis, F. Tombari, and N. Navab, "Deeper depth prediction with fully convolutional residual networks," in *2016 Fourth international conference on 3D vision (3DV)*. IEEE, 2016, pp. 239–248.
- [41] B. Lim, S. Son, H. Kim, S. Nah, and K. Mu Lee, "Enhanced deep residual networks for single image super-resolution," in *CVPR workshops*, 2017, pp. 136–144.
- [42] D. P. Kingma and J. Ba, "Adam: A method for stochastic optimization," *arXiv preprint arXiv:1412.6980*, 2014.
- [43] K. He, J. Sun, and X. Tang, "Guided image filtering," *IEEE transactions on pattern analysis and machine intelligence*, vol. 35, no. 6, pp. 1397–1409, 2012.
- [44] C. Ma, Y. Rao, Y. Cheng, C. Chen, J. Lu, and J. Zhou, "Structure-preserving super resolution with gradient guidance," in *CVPR*, 2020, pp. 7769–7778.
- [45] J. Liang, J. Cao, G. Sun, K. Zhang, L. Van Gool, and R. Timofte, "Swinir: Image restoration using swin transformer," in *CVPR*, 2021, pp. 1833–1844.
- [46] H. Wang, X. Chen, B. Ni, Y. Liu, and J. Liu, "Omni aggregation networks for lightweight image super-resolution," in *Proceedings of the IEEE/CVF Conference on Computer Vision and Pattern Recognition*, 2023, pp. 22378–22387.
- [47] L. Yang, B. Kang, Z. Huang, X. Xu, J. Feng, and H. Zhao, "Depth

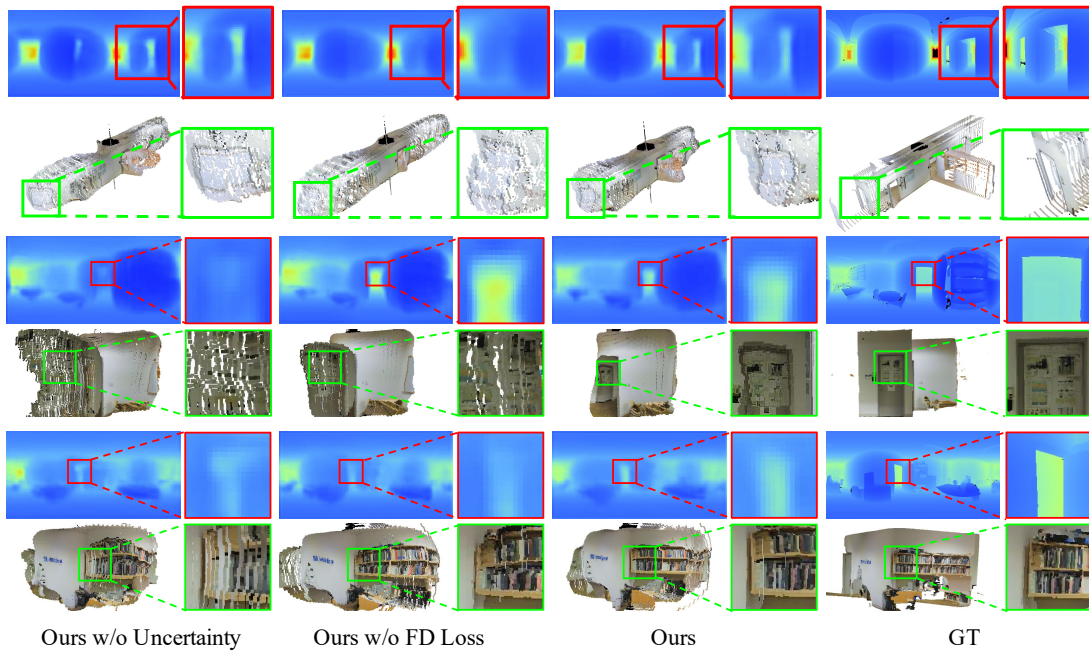
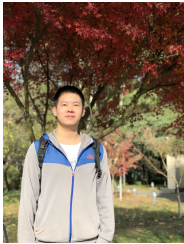


Fig. 15. Visual comparison of the impacts of uncertainty estimation in the ODI SR task and FD loss on the overall framework.

anything: Unleashing the power of large-scale unlabeled data,” *arXiv preprint arXiv:2401.10891*, 2024.

- [48] Y. Chen, S. Liu, and X. Wang, “Learning continuous image representation with local implicit image function,” *2021 IEEE/CVF Conference on Computer Vision and Pattern Recognition (CVPR)*, pp. 8624–8634, 2021.



Zidong Cao is a Ph.D. student in the Visual Learning and Intelligent Systems Lab, Artificial Intelligence Thrust, Guangzhou Campus, The Hong Kong University of Science and Technology (HKUST). His research interests include 3D vision (depth completion, depth estimation, etc.), DL (self-supervised learning, weakly-supervised learning, etc.), and omnidirectional vision.



Hao Ai is a Ph.D. student in the Visual Learning and Intelligent Systems Lab, Artificial Intelligence Thrust, Guangzhou Campus, The Hong Kong University of Science and Technology (HKUST). His research interests include pattern recognition (image classification, face recognition, etc.), DL (especially uncertainty learning, attention, transfer learning, semi-/self-supervised learning), and omnidirectional vision.



Athanasios V. Vasilakos is with the Center for AI Research (CAIR), University of Agder (UiA), Grimstad, Norway. He served or is serving as an Editor for many technical journals, such as the *IEEE TRANSACTIONS ON AI*, *IEEE TRANSACTIONS ON NETWORK AND SERVICE MANAGEMENT*, *IEEE TRANSACTIONS ON CLOUD COMPUTING*, *IEEE TRANSACTIONS ON INFORMATION FORENSICS AND SECURITY*, *IEEE TRANSACTIONS ON CYBERNETICS*, *IEEE TRANSACTIONS ON NANOBIOSCIENCE*, *IEEE TRANSACTIONS ON INFORMATION TECHNOLOGY IN BIOMEDICINE*; *ACM Transactions on Autonomous and Adaptive Systems*; the *IEEE JOURNAL ON SELECTED AREAS IN COMMUNICATIONS*. He is WoS highly cited researcher(HC).

IEEE TRANSACTIONS ON INFORMATION TECHNOLOGY IN BIOMEDICINE; *ACM Transactions on Autonomous and Adaptive Systems*; the *IEEE JOURNAL ON SELECTED AREAS IN COMMUNICATIONS*. He is WoS highly cited researcher(HC).



HCI), etc. For more about me, please visit <https://vlislab22.github.io/vlislab/>.

Lin Wang (IEEE Member) is an assistant professor in the AI Thrust, CMA Trust at HKUST, GZ, and an affiliate assistant professor in the Dept. of CSE, HKUST, CWB. He did his Postdoc at the Korea Advanced Institute of Science and Technology (KAIST). He got his Ph.D. (with highest honors) and M.S. from KAIST, Korea. He had rich cross-disciplinary research experience, covering mechanical, industrial, and computer engineering. His research interests lie in computer and robotic vision, machine learning, intelligent systems (XR, vision for